Journal of Anatolian Environmental and Animal Sciences
(*Anadolu Çevre ve Hayvancılık Bilimleri Dergisi*)
Doi: https://doi.org/10.35229/jaes.572713

JAES
Year: 4, No: 2, 2019 (230-242)
AÇEH
Yıl: 4, Sayı:2, 2019 (230-242)

ARAŞTIRMA MAKALESİ **RESEARCH PAPER**

Nudging Time-Scale Sensitivity of a Simplified Black Sea CIL Forcing with a Three-Dimensional Idealized Bosphorus Strait Hydrodynamic Model

Adil SÖZER[1*,2] Emin ÖZSOY[2]

[1]*Fatsa Faculty of Marine Sciences, Ordu University, Turkey*
:https://orcid.org/0000-0002-8674-1461
[2]*Institute of Marine Sciences, Middle East Technical University, Mersin, Turkey*
: https://orcid.org/0000-0002-1519-0471

Received date: *31.05.2018* ***Accepted date:*** *09.08.2019*

How to cite: ***Sözer, A. & Özsoy, E. (2019).*** Nudging Time-Scale Sensitivity of a Simplified Black Sea CIL Forcing with a Three-Dimensional Idealized Bosphorus Strait Hydrodynamic Model. *Anatolian Env. and Anim. Sciences, 4(2),* 230-242.
*Atıf yapmak için****: Sözer, A. & Özsoy, E. (2019***). Üç Boyutlu İdealize Bir İstanbul Boğazı Hidrodinamik Modelinde Karadeniz Soğuk Ara Tabakası Zorlamasının Zaman Ölçeği Hassasiyeti. *Anadolu Çev. ve Hay. Dergisi*, 4(2)**,** 230-242.

Abstract: In this study, hydrodynamics of the Bosphorus Strait is examined under idealized conditions with a three-dimensional numerical model. In particular, penetration of a simplified Cold Intermediate Layer (CIL) of the Black Sea into the Strait specified at the boundary is simulated with the aim of testing the sensitivity of the idealized model with respect to nudging strength. Successful penetration of a CIL-like stratification can only be achieved by inflowing nudging time-scales less than or equal to one day, while the outflowing nudging strength is found to be insignificant. However, numerical instabilities at the boundary are observed for strong nudging cases with tnudg ≤ 0.01 day, suggesting that a careful selection of the nudging time-scale is important to achieve successful simulations of the CIL even in this highly idealized setup of the Bosphorus strait. The presence of CIL altering the temperature distribution within the northern section of the idealized channel has a significant impact on the exchange through the strait. CIL reduces the density difference across the strait resulting in decreased layer fluxes and velocities, while a two-layer sense hydraulic control still holds at the sill.

Keywords: Bosphorus, cold intermediate layer, idealized 3D model, nudging at open boundary.

Üç Boyutlu İdealize Bir İstanbul Boğazı Hidrodinamik Modelinde Karadeniz Soğuk Ara Tabakası Zorlamasının Zaman Ölçeği Hassasiyeti

Öz: Bu çalışmada İstanbul Boğazı'nın hidrodinamiği üç boyutlu bir sayısal model kullanılarak idealize koşullar altında incelenmiştir. Karadeniz'in soğuk ara tabakasının (SAT) basitleştirilmiş bir halinin idealize modelin kuzey sınırından penetrasyonu simüle edilerek modelin açık sınır koşullarıyla gerçekleştirilen sıcaklık profili zorlamasının zaman ölçeğine (tnudg) hassasiyeti araştırılmıştır. SAT benzeri bir tabakanın boğaza penetrasyonu ancak bir günden küçük tnudg (sınırdan içeri) değerleri ile mümkün olmuş ve sınır-dışarı tnudg değerinin kuvvetinin önemsiz olduğu tespit edilmiştir. Bununla birlikte güçlü zorlama değerleri altında (tnudg ≤ 0.01) kuzey açık sınırında sayısal düzensizlikler meydana gelmiştir, bu da oldukça idealize edilmiş bir Boğaz modeli için bile SAT'ın başarılı simülasyonlarını için zorlama zaman ölçeğinin dikkatlice seçilmesi gerektiğini göstermektedir. İdealleştirilmiş kanalın kuzeyindeki sıcaklık dağılımını değiştiren SAT'ın varlığı, iki tabakalı değişim akımı üzerinde önemli bir etkiye sahiptir. Boğaz'ın kuzey kısmındaki stratifikasyonun değişimi ile kanalın iki ucu arasındaki yoğunluk farkı ve buna istinaden alt ve üst tabaka akıları ve hızları azalmış olmakla birlikte, iki tabakalı yaklaşıma dayanan kuzey eşiğindeki hidrolik kontrol kaybolmamıştır.

Anahtar sözcükler: İstanbul boğazı, soğuk ara tabaka, idealize 3D model, açık sınır zorlama

INTRODUCTION

Geographical Setting: The Turkish Straits System (TSS) is a restricted pathway of water exchange between the Mediterranean and Black Sea, connecting them with the Sea of Marmara respectively through the narrow Straits of Dardanelles and Bosphorus. The Sea of Marmara located in the middle has a surface area of 11,500 km^2. Both straits have sinuous bends and turns along the way, with deep cut channels and topographic barriers adjoining steep topography. The Dardanelles Strait is ~75 km long with a minimum width of 1.3 km, while the Bosphorus Strait, the most constricted part of the TSS pathway, has a total length of ~35 km and width varying between 700 m and 3500 m. The bathymetry of the Bosphorus Strait is extremely variable in both along and cross-channel directions with a maximum depth of ~105 m coinciding with the narrowest (contraction) part of the strait located at one-third of the length of the strait from the south end (Marmara junction). A sill is located outside the Black Sea exit and inside a canyon extension of the Bosphorus Strait. The contraction and sill are the two prominent topographic barriers of the Bosphorus that have determining influence on the exchange through the strait (Figure 1).

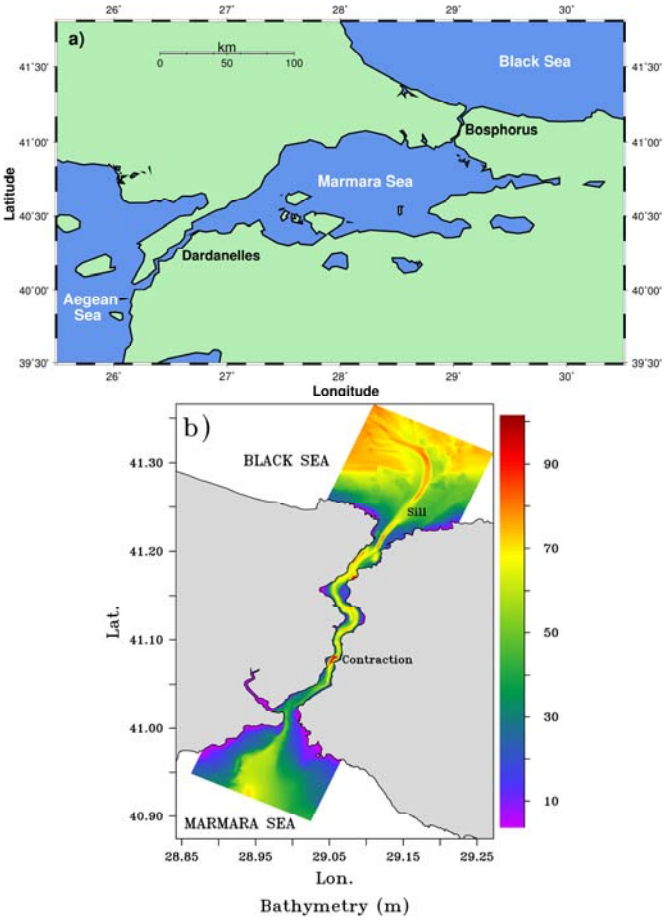

Figure 1. a) Location map showing Turkish Straits System and b) bottom topography of the Bosphorus Strait.

Fluxes: TSS is a two-layer stratified (Andersen & Carmack, 1984; Ünlüata et al., 1990) water path between the Black Sea and the Mediterranean Sea, with a sharp interface at 25 m separating water masses originating from neighboring basins. The density difference between layers is characterized by an extreme ratio of $\Delta\rho/\rho=10^{-2}$. The wind-mixed upper-layer responds to seasonal changes, while the TSS lower-layer with relatively uniform properties buffers inputs from the Aegean Sea (Beşiktepe et al., 1993, 1994, 2000). The two-layer exchange through the TSS transmits environmental signals such as eutrophication and marine pollution between the adjacent Black and Mediterranean Seas. Because it is located in a region of climatic contrasts (Özsoy & Ünlüata, 1997; Özsoy, 1999), the TSS has a strong influence on the long-term trends and stability of these basins. Buoyancy transport through the Bosphorus Strait, surface fluxes and freshwater inputs by major rivers control the stratification in the Black Sea. Detailed knowledge of this transport (Oğuz et al., 1990; Ünlüata et al., 1990; Gregg et al., 1999; Gregg & Özsoy, 1999, 2002) has fundamental importance for regional climate.

The driving mechanism of the two-layer exchange through the Bosphorus Strait is gravity, producing hydrostatic pressure difference between two ends of the strait, favoring subsurface flow of dense water of Mediterranean origin towards the Black Sea and compensating surface flow towards the Marmara Sea of less dense Black Sea waters. The excess of fresh water supply in the annual water budget of the Black Sea results in superior sea-level on the Black Sea side on the average, creating a net flux towards the Marmara Sea and the Mediterranean in general. The first experimental verification of the two-way exchange at the Bosphorus Strait, based on measurements and laboratory demonstration by Marsili, (1681) constituted the very beginnings of ocean science (Defant, 1961; Soffientino & Pilson, 2005; Pinardi, 2009; Pinardi et al., 2018).

A high resolution, three-dimensional description of the flow has been provided at Bosphorus by Gregg et al., (1999), Özsoy et al., (2001) and Gregg and Özsoy (2002). The along-channel variation of the salinity, temperature and the velocity fields through the strait display non-linear, abrupt changes by hydraulic adjustments in accordance with changes in channel cross-section (at the south-exit, contraction and the north-sill) according to Özsoy et al., (1998). Using salinity as a conservative tracer, sharp adjustments in properties have been detected at the north-sill, contraction and exit sections by Latif et al., (1991), Özsoy et al., (2001) and Gregg and Özsoy (2002). Between these rapid adjustment regions, linear variations occur in water properties of each layer, separated by an interfacial mixing layer that is about 10 m thick. The offset between along-channel velocity and salinity, with the zero-velocity isotach lying slightly below the salinity interface at the south end of the strait and above it at the north end, as proposed by

Tolmazin (1985), has been verified through intensive measurements of Gregg and Özsoy (2002) and model results of Sözer (2013).

The sharp pycnocline descending from near-surface depth at the south-exit towards the bottom at the north-sill is modulated by seasonal changes in the neighboring seas. On the southern side, a permanent two-layer stratification exists in the Marmara Sea, with the halocline at relatively constant depth of 25 m. Seawater with average temperature and salinity values of ~14.5 ºC and ~38.5 fills the basin below the halocline, with almost constant properties throughout the year. The ambient upper layer of the Marmara Sea near the Bosphorus exit exhibits a typical salinity range of 20 to 25 and temperatures from 7 ºC to 22 ºC depending on season (Özsoy et al., 1986, 1988; Ünlüata et al., 1990; Beşiktepe et al., 1994). The surface salinity on the Black Sea side varies within 16-18 directly related to the fresh water inflow and air-sea fluxes, while surface temperature has a much wider range of 4 ºC - 25 ºC. The vertical profile of ambient Black Sea salinity can be considered to be uniform till the north-sill depth, while the most significant feature in temperature is the well-known permanent cold intermediate layer (CIL) of the Black Sea formed in winter with minimum core temperatures of about 6.5 ºC becoming as shallow as 25 m in summer and reaching the shelf bottom at the northern end of the Bosphorus in winter (Ovchinnikov & Popov, 1991; Özsoy et al., 2001). Therefore stratification predominantly exists in temperature rather than salinity at these depths, with the CIL overtopped by the shallow mixed-layer in summer.

The average annual water balance of the Black Sea, calculated as Precipitation (P) + River Runoff (R) - Evaporation (E) = 300 + 352 - 353 = ~300 km^3/yr ought to be balanced by the Bosphorus net flux in the same amount, also in the climatic sense. Average salinity at junctions of the TSS (Özsoy et al., 1986; 1988) and the water balance of the Black Sea have been used to compute horizontal layer and vertical entrainment fluxes of the TSS regions based on the Knudsen mass conservation equations (Ünlüata et al., 1990), updated later to yield seasonal estimates (Tuğrul et al., 2002). These estimates provide annual averages of Q_1 = ~650 km^3/yr transported by the upper-layer outward from the Black Sea and and Q_2 = ~330 km^3/yr into the Black Sea by the lower layer. According to current meter and ADCP velocity profile measurements, seasonal variations were found in ranges of Q_1 = 450-856 km^3/yr and Q_2 = 226-432 km^3/yr respectively for the upper and lower layers. Transient events are recorded with maximal instantaneous fluxes of ~1600 km^3/yr and ~650 km^3/yr with short-term blocking of the flows in either layer (Ünlüata et al., 1990; Latif et al., 1991; Özsoy et al., 1995, 1996, 1998, 2001; Özsoy & Ünlüata, 1997, 1998; Jarosz et al., 2011a,b; Altıok & Kayışoğlu 2015), reviewed in Schroeder et al., (2012) and Jordà et al., (2017).

Controlled Flows: Armi (1986) introduced hydraulic analysis of two-layer, inviscid, uniform, one-dimensional flows through channels with gradually varying geometry, where the Froude-number (F^2) for each layer and the two-layer composite Froude-number G^2 are the relevant parameters. A "hydraulically controlled" solution is obtained in the neighborhood of a critical point, where a regularity condition leads to the requirement that G^2=1. These controlled solutions are unique for a given channel geometry, density difference and a net-flow rate, enabling to analyze the two-layer system flowing through a contraction. Further analysis by Farmer & Armi (1986) of two-layer flow through the combination of a sill and a contraction showed that a "maximal-exchange" solution is obtained in the case of a sill located between the contraction and the lighter water reservoir. Maximal-exchange theory has been further extended to cover time-dependence (Helfrich, 1995) and non-rectangular cross-sections (Dalziel, 1991), and later to three-layer (Smeed, 2000) and multi-layer (Lane-Serff et al., 2000) flows. Other analytical or numerical studies have covered aspects of bottom friction (Pratt, 1986), dissipation and mixing (Hogg et al., 2001; Winters & Seim, 2000), lateral variations in layer velocities and thicknesses (Pratt, 2008) and vertical velocity shear (Garrett & Gerdes, 2003).

In the case of the Bosphorus, the northern sill and the mid-strait contraction serve as the main topographic features supporting hydraulic controls. With ideally located contraction and sill between suitable reservoir conditions, the Bosphorus is ideally suited to support 'maximal-exchange' regime (Özsoy et al., 2001). Maximal-exchange has been demonstrated through modelling (Sözer & Özsoy, 2017), subject to possible controls at the south-exit, contraction and the north-sill, yielding unique solutions for specified density difference between two ends and net barotropic flux through the strait. However, any one of these hydraulic controls may be drowned by existing stratification at the reservoirs when exceptionally large barotropic fluxes are imposed in either direction.

Three-dimensional models solving the full set of primitive equations have been developed for simplified hydrography and geometry of the Bosphorus Strait (Sözer & Özsoy, 2002; Oğuz, 2005). Some observed features, including hydraulic transitions and blocking of the flow in either direction (Latif et al., 1991), sharp changes of free-surface elevation at the contraction (Gregg et al., 1999; Gregg & Özsoy, 2002), and the separation of the zero-velocity line with the pycnocline (Tolmazin, 1985; Gregg & Özsoy, 2002) have been demonstrated by the above models. A recent progression of three-dimensional numerical models have explored the effects of high resolution bottom topography of Bosphorus Strait (Öztürk et al., 2012; Sözer & Özsoy, 2017), enlarged computational domain to include complete TSS (Sannino et al., 2017; Aydoğdu et al., 2018) or the adjacent Black and Aegean Seas (Stanev et al., 2017).

In the present study, hydrodynamics of the Bosphorus Strait is examined under an idealized model configuration. In particular, we examine the influence of the Cold Intermediate Layer (CIL) characteristics (Ovchinnikov

& Popov, 1991; Altıok et al. 2012) specified at the Black Sea end of the Strait with the aim of testing the sensitivity of the idealized model with respect to nudging strength.

MATERIAL and METHOD

Description of the Numerical Model (ROMS): The regional Ocean Modeling System ROMS (www.myroms.org) is an open source community ocean model based on primitive equations, extended model physics and parameterizations (Haidvogel et al., 2000; Wilkin et al., 2005; Hedström, 2009). It is a modular code written in F90/F95 powered with C-preprocessing to activate or deactivate various options prior to compilation. The model has the ability of running in parallel mode on a network of multi-core computers utilizing the MPI (Message passing interface) standard.

ROMS uses a staggered vertical grid discretized by terrain-following coordinates adapted to variable topography (Song & Haidvogel, 1994). It uses an Arakawa C-grid in the horizontal plane and works on either rectilinear or boundary-fitted orthogonal curvilinear grids with an available land mask option for delineating coastal boundaries. Its split-explicit kernel solves the fast barotropic (external) mode coupled with the slower baroclinic (internal) mode.

There are several options available for high-order tracer and momentum advection schemes. Laplacian and biharmonic horizontal viscosity and diffusion coefficients can either be set or estimated by the Smagorinsky (1963) method. To avoid spurious vertical mixing in the presence of sharp topography, ROMS has options for mixing on constant geo-potential or constant potential density surfaces. In addition, to constant vertical viscosity and diffusion, options for local, Mellor and Yamada (1982) and Generic Length Scale (GLS) (Umlauf & Burchard, 2003) or nonlocal, K-Profile boundary layer (Large et al., 1994) parametrizations are available for comparative evaluations (Warner et al., 2005; Durski, 2004).

Among the various open boundary conditions used in ROMS, persistence and gradient boundary conditions are available in addition to the Orlanski radiation boundary condition where disturbances are radiated out with local phase speed (Orlanski, 1976; Raymond & Kuo, 1984) or defined by a mixed radiation and nudging formula where nudging time scales can be separately set for inflow and outflow conditions (Marchesiello et al., 2001).

Implementation of the model to the Bosphorus Strait: The idealized geometry of the Bosphorus Strait consists of a ~35 km long channel of rectangular cross-section with abrupt openings at the two ends opening into wider channels of 5100 m width, representing the Black Sea and the Marmara Sea reservoirs. A symmetric contraction of about 4 km length occurs at about one-third of the length of the strait from the south end, where the width of the channel decreases from 1300 m to 700 m at the narrowest section. A sill of 1 km length and 13 m height at the crest of a Gaussian shape is specified just before the north end of the channel. Detailed layout of the idealized domain is demonstrated in Figure 2, emphasizing the primary geometric features of the Bosphorus, i.e. the contraction, north-sill and the south-exit.

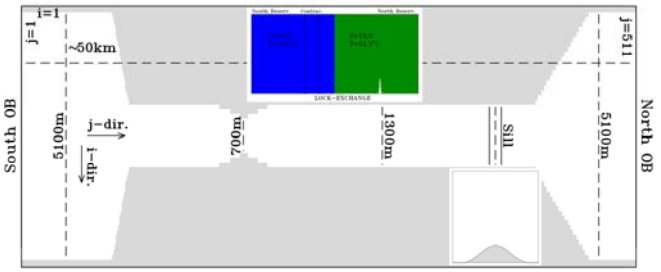

Figure 2. Layout of the idealized Bosphorus Model and the Lock-Exchange (LE) initial condition demonstrated in top insert.

The model domain is discretized with a rectilinear grid of 55*512 grid points of spacing dx=dy=100m in the horizontal and 35 topography following s-levels resulting in a vertical resolution of dz=1.6 - 2.0 m. The channel geometry is formed by masking of the grid cells. With this setup, the highly complex geometry of the Bosphorus Channel is represented in a simplified manner including only the essential geometric features of the strait; contraction, north sill and south exit which have the primary influence on the strait exchange flow.

RESULTS and DISCUSSION

In this section, the configuration details for the central simulation and the nudged cases are presented first and followed by an overview of the central case under the BASE_INI title. Finally, the results of the nudged solutions for the two groups of simulations (with OBCFAC=1 and with different OBCFAC values) are discussed in the last two subsections.

Central Simulation: The first and central case of the study is a lock-exchange simulation (hereinafter referred as "BASE_INI"), very similar to the one used by Sözer & Özsoy, (2017). The initial lock-exchange condition consists of two different water masses of contrasting properties at rest and meeting at the mid-channel, where the water properties are based on the in-situ data presented by Gregg & Özsoy (2002) from September 1994, with S (Salinity) = 38.0, T (Temperature) = 13.0 ^{o}C and S = 17.6, T = 24.1 ^{o}C at the south and north reservoirs respectively, (demonstrated in Figure 2).

MY2.5 turbulence closure with Smagorinsky-like harmonic viscosity and diffusivity along geo-potential surfaces is utilized for the vertical and horizontal directions respectively. No-slip boundaries are assumed at the side-walls and a quadratic bottom friction with RDRG2=0.005 is implied at the bottom, while all surface fluxes are set to zero. Both two and three-dimensional model variables including the turbulent kinetic energy fields are treated with the

radiation boundary conditions except for the north-south component of the barotropic velocity, persisted at the south edge to provide constant barotropic volume-flux of ~3500 m^3/s through the channel. This value is comparable to the average value of 300 $km^3/yr \approx 9460\ m^3/s$ estimated by Ünlüata et al., (1990), but more conformable to the milder conditions of September 1994 given by Gregg & Özsoy (2002). The volume conservation switch is activated at the south and the north open boundaries. MPDATA advection scheme is selected for salinity and temperature due to sharp gradients of the lock-exchange initialization, while default numerics are used for the advection of momentum. Considering that the internal Rossby Radius of Deformation is significantly larger than the channel and the reservoir widths of the idealized channel, the rotation of the earth is ignored. A baroclinic time-step of 3.5 seconds and barotropic step-size that is 20 times smaller is used to ensure stable integrations. Total duration of the BASE_INI simulation is ~1 day which is long enough to reach steady-state solutions.

Nudged Simulations: The first group of simulations consists of six cases restarted from the steady-state BASE_INI solution with temperature and salinity applied at the north end simulating Black Sea water properties. In particular, a simplified temperature profile representing the CIL is applied with uniform values near the surface (T=24.1 ºC) and the bottom (T=13.0 ºC), with linear thermocline variation between 22 - 44 m (Figure 3a). The temperature forcing is applied with a mixed radiation and nudging boundary condition at the north end of the model domain, while the salinity at the two open boundaries and the temperature at the south boundary are set to radiate freely as in the case of BASE_INI configuration. Cumulative duration of the nudged simulations are about eight days with the nudging time-scales (tnudg) of 100.0, 10.0, 1.0, 0.1, 0.01, 0.001 days for both the inflowing and the outflowing conditions as presented in the Table 1.

Table 1. Simulations forced with a CIL-like temperature profile at the north open boundary initialized from the BASE_INI solution with different nudging time-scales. The ratio between nudging time scales of the passive (outflow) and active (inflow) open boundary conditions is equal 1 (OBCFAC=1) in these cases.

Simulation	Inflow nuding time scale (tnudg in) (Days)	Outflow nudging time scale (tnudg out) (Days)
TN100	100	100
TN10	10	10
TN1	1	1
TN01	0.1	0.1
TN001	0.01	0.01
TN0001	0.001	0.001

In the second group, three extra simulations are performed to test the effect of nudging time scale for outflowing boundary conditions. In these simulations, the outflow nudging time-scale (tnudg out) is varied from 5.0 days to 100.0 days while the inflow nudging time-scale is held constant at 0.1 day as in TN01 acting as control case which is selected according to the results of the first group of simulations. Similar to the previous group, the total duration of these simulations is ~8 days.

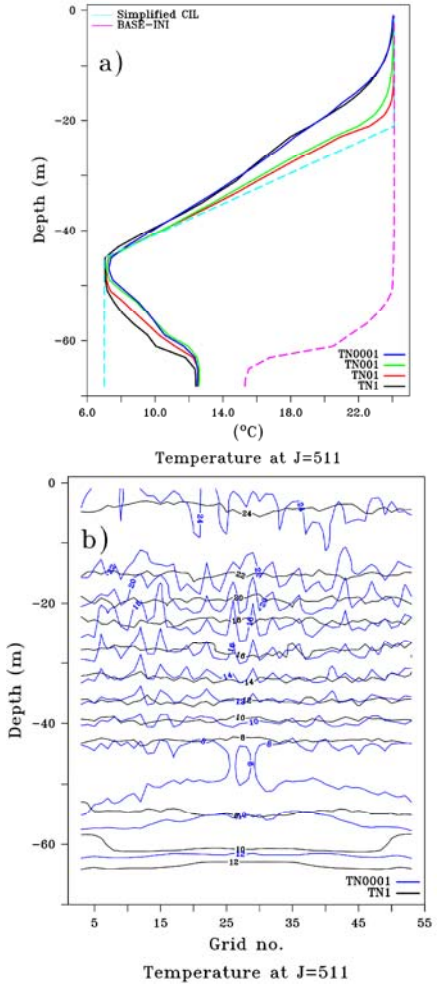

Figure 3. a) Model temperature profiles next to the north boundary (averages across channel width at section j=511, at the end of the simulation) obtained for the last four experiments of Table 1, compared with the simplified CIL temperature profile (dashed light blue) and the initial condition obtained from the BASE_INI (dashed, purple) simulation at steady-state and b) cross-channel contour plot at the same grid section for the two solutions with longest and shortest nudging time-scales among these four cases.

BASE_INI Solution: The present, BASE_INI setup is a modified version of the idealized setup discussed in detail by Sözer (2013) and Sözer & Özsoy (2017) (hereinafter referred as "BASE"). The present solutions however, are quite different due to the CIL boundary conditions applied at the north end and differences in mixing parameterizations. A detailed analysis of the BASE_INI solution will not be given here, but a brief comparison with BASE solution of Sözer & Özsoy (2017) follows below. The use of MY2.5 closure in the BASE_INI case significantly altered the vertical structure, resulting in a thicker interfacial layer. The bottom friction is still weak, as in the case of BASE solution. The total lateral resistance at solid walls in the present case is smaller than obtained in our earlier model,

due to Smagorinsky diffusivity applied near the no-slip boundaries. In consequence to decreased friction, the adjustment is faster and convergence to steady-state is obtained by the end of first day. As a result of decreased friction, water exchange and layer fluxes are significantly larger than the BASE case resulting in an increased two-layer exchange. Almost linear changes are evident in tracer and velocity fields as a function of distance along the main part of the channel, while sharp hydraulic adjustments occur at topographic barriers of the sill and contraction regions. Steady-state along-channel responses of temperature, salinity, density and velocity of BASE_INI can be visualized in the comparison figures (Figure 4 and Figure 5) given in the context of the next section.

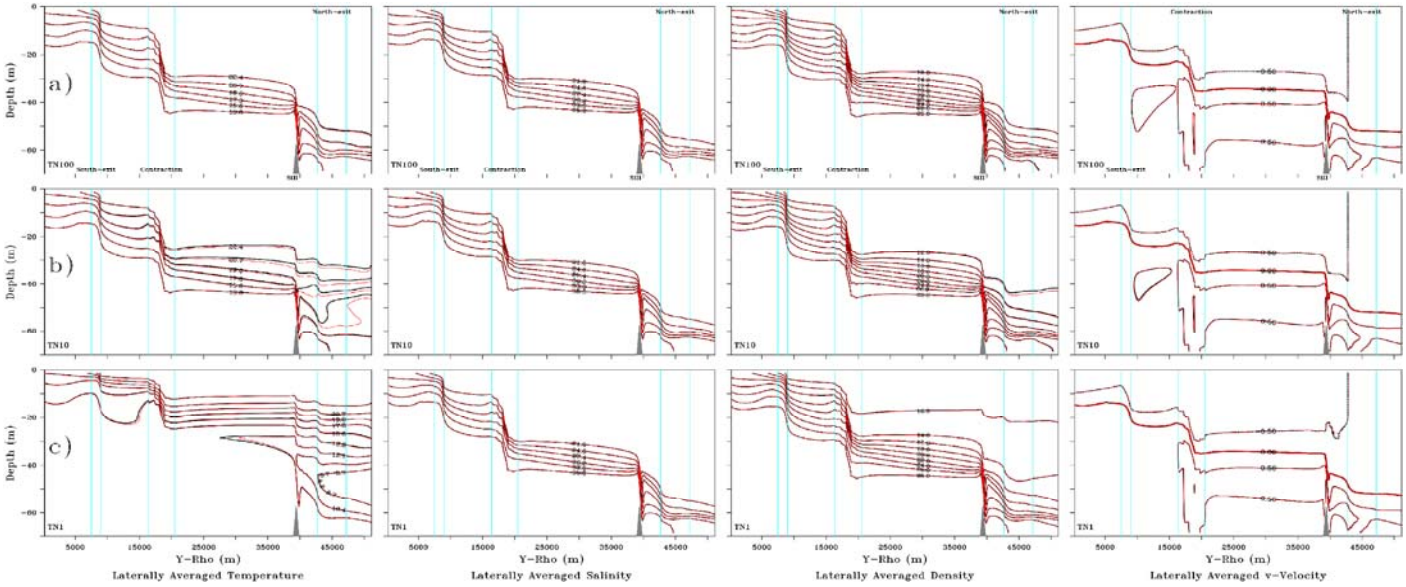

Figure 4. Along channel comparison of the BASE_INI (black) solution with the nudged (red) solutions of Table 1; a) TN100, b) TN10 and c) TN1; in terms of laterally averaged temperature, salinity, density and v-velocity responses, same contour levels are used for the BASE_INI and nudged solutions, location of the topographic changes are marked by light blue lines.

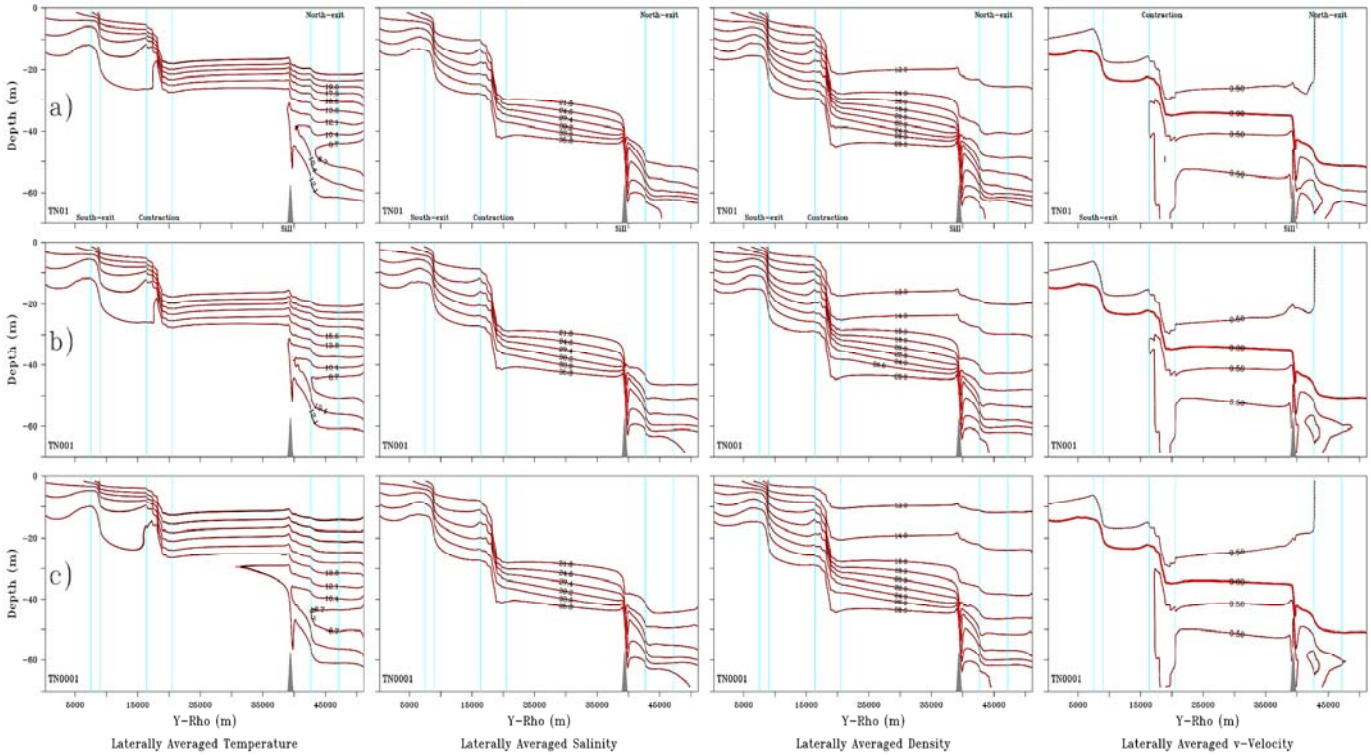

Figure 5. Along channel comparison of the BASE_INI (black) solution with the nudged (red) solutions of Table 1; a) TN01, b) TN001 and c) TN0001; in terms of laterally averaged temperature, salinity, density and v-velocity responses, same contour levels are used for the BASE_INI and nudged solutions, location of the topographic changes are marked by light blue lines.

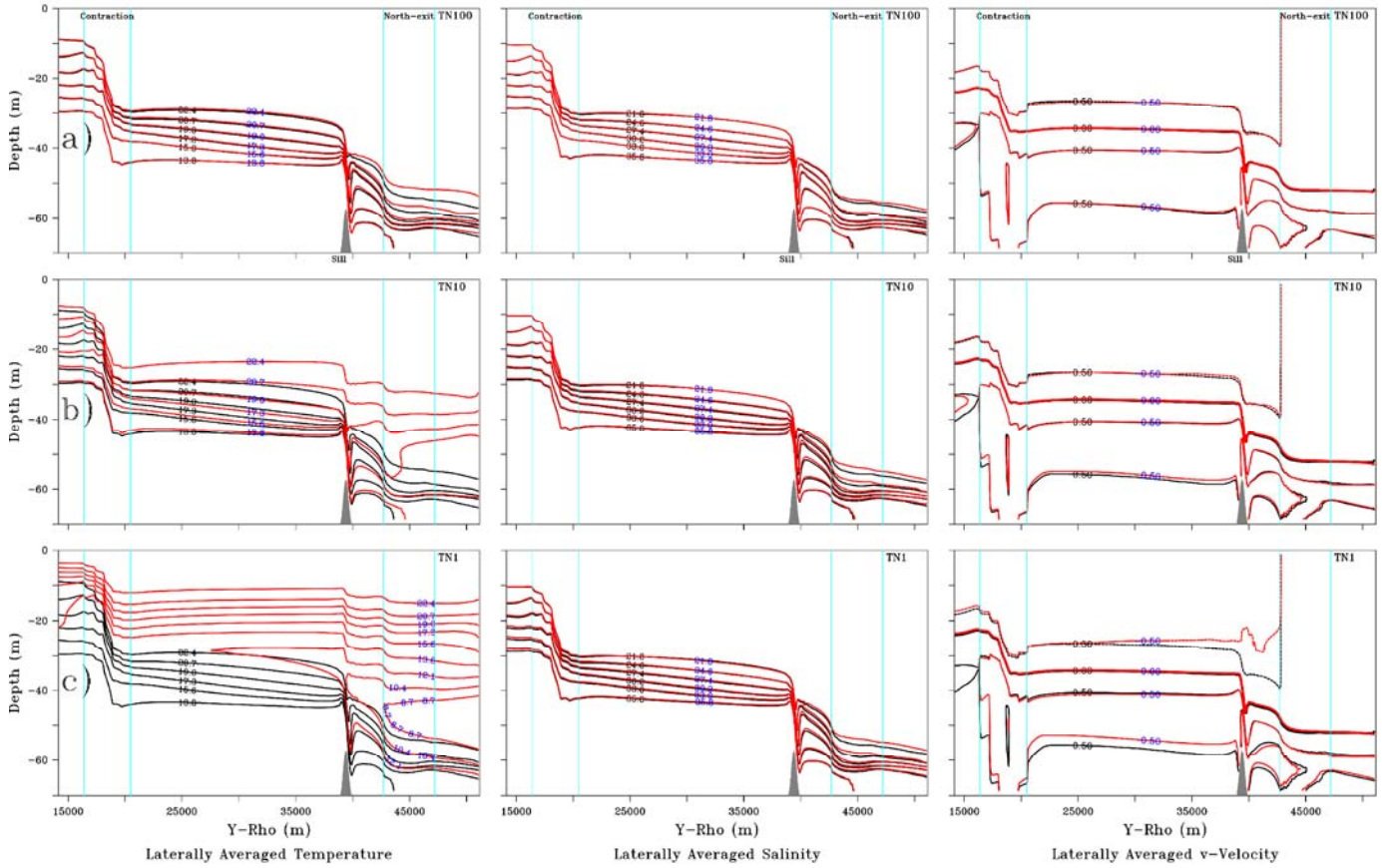

Figure 7. Evolution of the along-channel laterally averaged temperature, salinity and v-velocity responses (from the south of the contraction to the north end) for the last two time-levels corresponding to a duration of 0.81day for the cases a) TN100, b) TN10 and c) TN1, same contour levels are used for all cases, location of the topographic changes are marked by light blue lines.

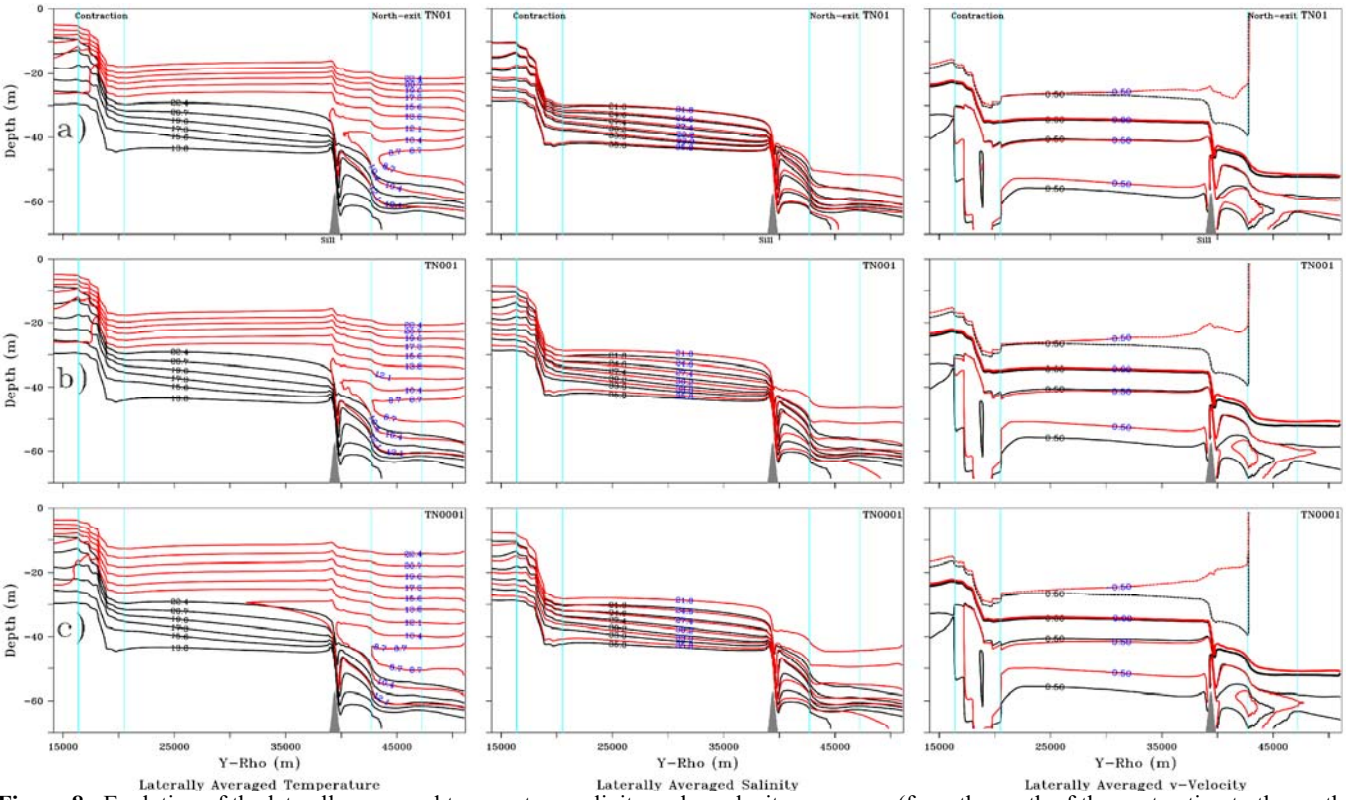

Figure 8. Evolution of the laterally averaged temperature, salinity and v-velocity responses (from the south of the contraction to the north end) for the last two time-levels corresponding to a duration of 0.81 day for the cases a) TN01, b) TN001 and c) TN0001, same contour levels are used for all cases, location of the topographic changes are marked by light blue lines.

Nudged Solutions with OBCFAC=1: In Figures 4 and Figure 5, the initial and the final state comparison of the along-channel laterally averaged temperature, salinity, density and north-south velocity (v-velocity) responses for the six nudged solutions of Table 1 are demonstrated. We see that for the two cases with tnudg ≥ 10.0 (tnudg referring both tnudg in and tnudg out when OBCFAC=1), nudging at the open boundary remains too weak to force the CIL into the model domain. Especially for the case TN100, the boundary condition is almost completely ineffective in modifying the already formed temperature stratification of the BASE_INI solution at the north boundary. For these six simulations, a steady-state solution is achieved not only in terms of energy and volume conservation (Figure 6) but also the model fields at the end of eight days suggest perfect invariability for the salinity and the velocity fields with only negligible changes in the temperature close to the north boundary (Figures 7 and Figure 8) except for the case TN10 where a relatively significant variation of the temperature field is observed within the northern section of the domain between the last two time-levels of the model output corresponding to a duration of 0.81 day. This is probably due to the indecisiveness of the boundary forcing for this simulation with a nudging time-scale which is neither strong nor completely weak, accordingly, although this solution has an altered temperature stratification within the north reservoir, it is significantly different than the tongue-like CIL penetration observed in the Bosphorus Strait (Gregg et al., 1999; Altıok et al., 2012).

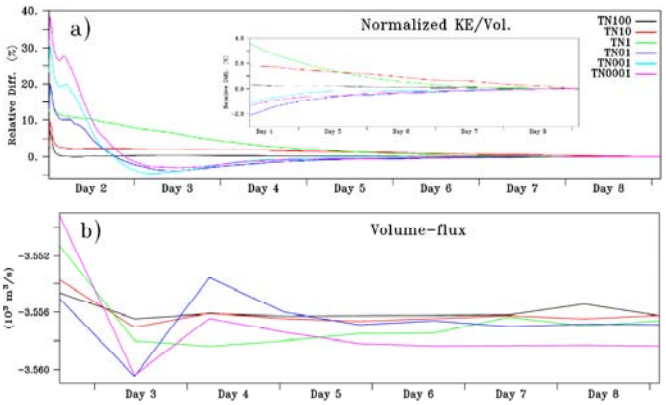

Figure 6. Time evolution of a) kinetic energy per volume relative to the final state and b) net volume-flux at a mid-strait section for the six nudged cases of Table 1.

For the simulations with tnudg ≤ 1.0 (TN1, TN01, TN001 and TN0001), in response to forced CIL profile along the northern boundary, the temperature interface along the channel has been tilted upwards. A tongue like along-channel penetration of the CIL is clearly shown in the temperature field for these four cases, Figure 4c and Figure 5, similar to observations and modeling studies (Gregg et al., 1999; Sannino et al., 2017). We observe that the along-channel CIL penetration modifies the v-velocity but can only weakly alter the position of the zero velocity surface. The resultant laterally averaged temperature profiles for these four simulations next to the north boundary (j=511) is given in Figure 3a together with the initial stratification and the nudged CIL-like temperature profile. Temperature profile at the neighborhood of the north open boundary (j=511), conforms to the boundary forcing for the inflowing upper-layer, but displays a solution between the initial state and the forced profile starting from the depth of 50m and gradually gets closer to the initial state with increasing depth for the outflowing lower-layer region. The success of the model in forcing the CIL profile within the inflowing section of the boundary depends on the nudging strength with a nonlinear behavior. For solutions TN01 and TN001 steady-state temperature response at the boundary conforms to the forced CIL-like profile quite well within the inflowing upper layer part, however for the simulations TN1 and TN001 which are the weakest and the strongest nudging cases, model response at the boundary at least slightly deviates from the forced CIL-like profile, Figure 3a.

Resultant cross-channel section of the temperature next to north boundary (j=511) are displayed for TN1 and TN0001, weakest and the strongest nudging cases among the four simulations, where the penetration of the CIL is successfully realized, Figure 3b. For the stronger nudging case, TN0001, the temperature cross-section is quite noisy within the inflowing upper layer region. Temperature responses for the cases TN01 and TN001 are not displayed in Figure 3b for the readability of the figure, but the unstable characteristic at the boundary become stronger with decreasing tnudg value (for stronger nudging). This is probably the cause of the unexpected thickening of the salinity interface within the north reservoir for the cases with tnudg ≤ 0.01, Figure 5b,c. For TN1 and TN01 which are the weaker nudging cases of these four simulations, noisy response at the boundary is at a relatively reasonable level and the thickening of the salinity interface is not observed.

Resultant cross-channel section of the temperature next to north boundary (j=511) are displayed for TN1 and TN0001, weakest and the strongest nudging cases among the four simulations, where the penetration of the CIL is successfully realized, Figure 3b. For the stronger nudging case, TN0001, the temperature cross-section is quite noisy within the inflowing upper layer region. Temperature responses for the cases TN01 and TN001 are not displayed in Figure 3b for the readability of the figure, but the unstable characteristic at the boundary become stronger with decreasing tnudg value (for stronger nudging). This is probably the cause of the unexpected thickening of the salinity interface within the north reservoir for the cases with tnudg ≤ 0.01, Figure 5b,c. For TN1 and TN01 which are the weaker nudging cases of these four simulations, noisy response at the boundary is at a relatively reasonable level and the thickening of the salinity interface is not observed.

Among these for simulations, TN01 can be considered as the most successful solution in terms of realization of the CIL intrusion to the strait while keeping numerical instabilities at the north open boundary at a reasonable level. For this simulation, the basin average density for the north reservoir is calculated as 1014.8 kg/m^3 which is greater than the value of the initial condition of 1013.0 kg/m^3 resulting in a decrease of density difference ($\Delta\rho$) between the reservoirs provided by the inclusion of the CIL only. A decrease in $\Delta\rho$ resulted in reduction of the layer fluxes through the channel as plotted in Figure 9a and layer averaged velocities as well. Volume-flux estimation at the mid-section between contraction and the sill, demonstrates roughly 6% decrease in both layers. The free-surface elevation difference between the two ends of the channel, $\Delta\eta$, of 38.1cm given by the BASE_INI solution decreases to 36.3cm with the intrusion of the CIL, which is an expected result, since the same specified volume-flux can now be possible with a smaller $\Delta\eta$ due to the decreased $\Delta\rho$. Between the contraction and the sill, the depth of the zero velocity surface preserves its initial position not only for this case but even for the simulations with considerably altered salinity stratification within the north reservoir which resulted in further decrease of $\Delta\rho$ across the strait. Although the layer fluxes and velocities decrease with decreasing $\Delta\rho$, the response of the zero velocity surface is insignificant and limited to the region between the sill and the north open boundary. The hydraulic response in terms of two-layer Froude-numbers (Armi, 1986) is demonstrated in Figure 9b and 9c. We see that, the BASE_INI and the TN1 solutions display significant differences only in actively flowing lower-layer Froude-number (F_2^2) within the north side of the channel. A considerable decrease in F_2^2 over the sill for the cases with tnudg $\leq$ 1.0 is observed, but even for the strongest nudged solution, TN0001, having the weakest lower-layer currents, energy corrected F_2^2 estimation (Sözer, 2013; Sözer & Özsoy, 2017) suggests a controlled lower-layer over the sill.

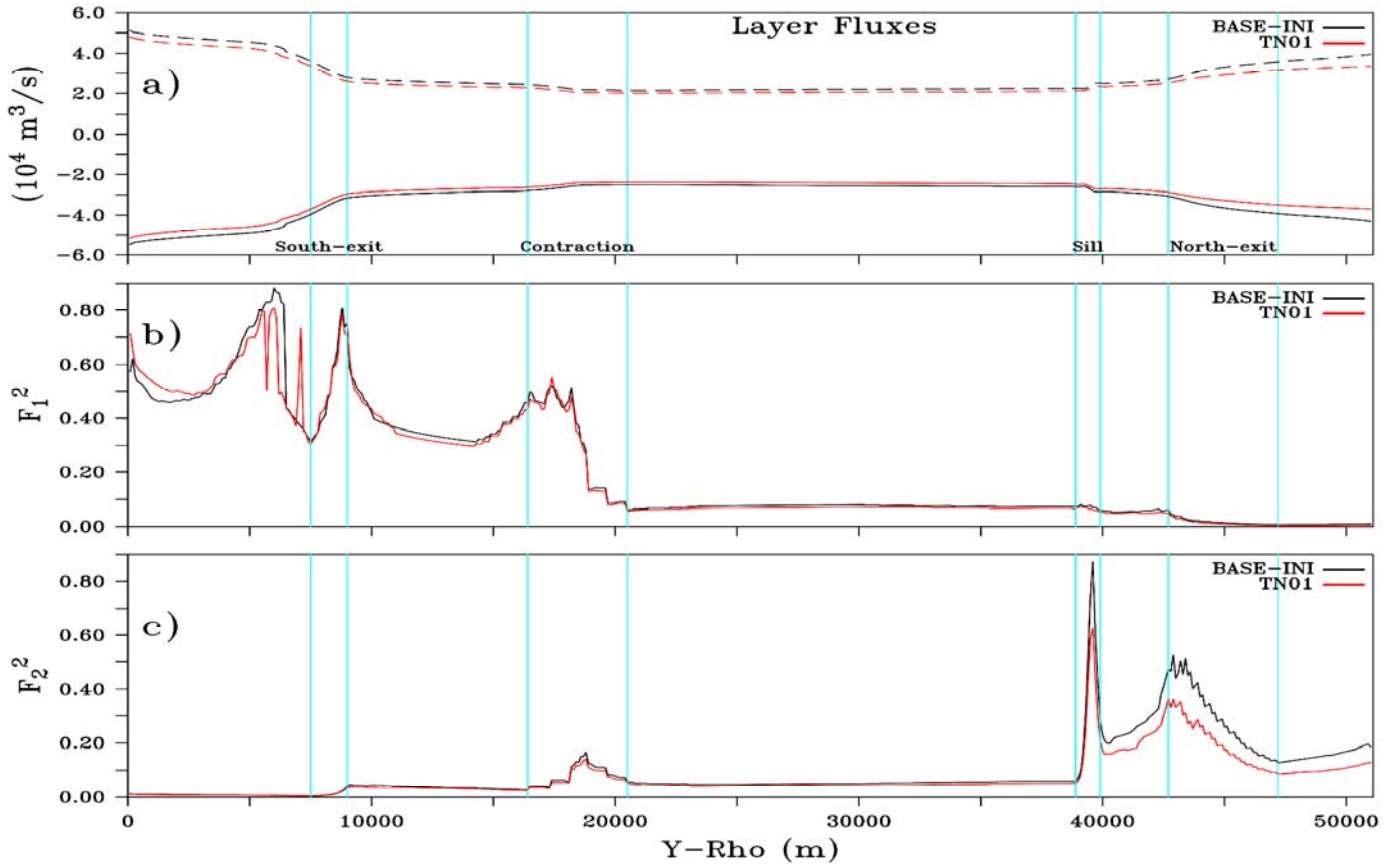

Figure 9. Along-channel variation of the a) upper and lower layer fluxes, Q_1 (solid) and Q_2 (dashed) respectively, and the Froude-number responses for the b) upper-layer; c) lower-layer based on the two-layer approximation defined by the zero v-velocity surface for the cases BASE_INI and TN01, location of the topographic changes are marked by light blue lines.

Nudged Solutions with different OBCFACs: In the previous section, the strength of the nudging is kept constant for the inflowing and the outflowing boundary conditions for all the nudged solutions of Table 1. We have seen that, for the cases with tnudg $\leq$ 1.0, steady-state solutions are obtained while preserving a CIL-like stratification proper to the forced profile within the northern section of the domain. The second set of simulations given in Table 2 are performed to

investigate effects of the outflow nudging strength of the applied CIL-like temperature boundary condition.

For the three simulations given in Table 2 together with the TN01 (as the control simulation) of the first group, along-channel salinity, temperature and v-velocity responses are displayed in Figure 10. Despite some minor differences, especially in the temperature field, the solutions are almost in perfect agreement for the simulations with different outflowing nudging time-scales.

Table 2. Simulations forced with a CIL-like temperature profile at the north open boundary initialized from the BASE_INI solution with variable outflow nudging time-scales (tnudg_out).

Simulation	Inflow nudging time-scale (tnudg_in) (*Days*)	Outflow nudging time-scale (tnudg_out) (*Days*)
TN100	0.1	5
TN10	0.1	50
TN1	0.1	100

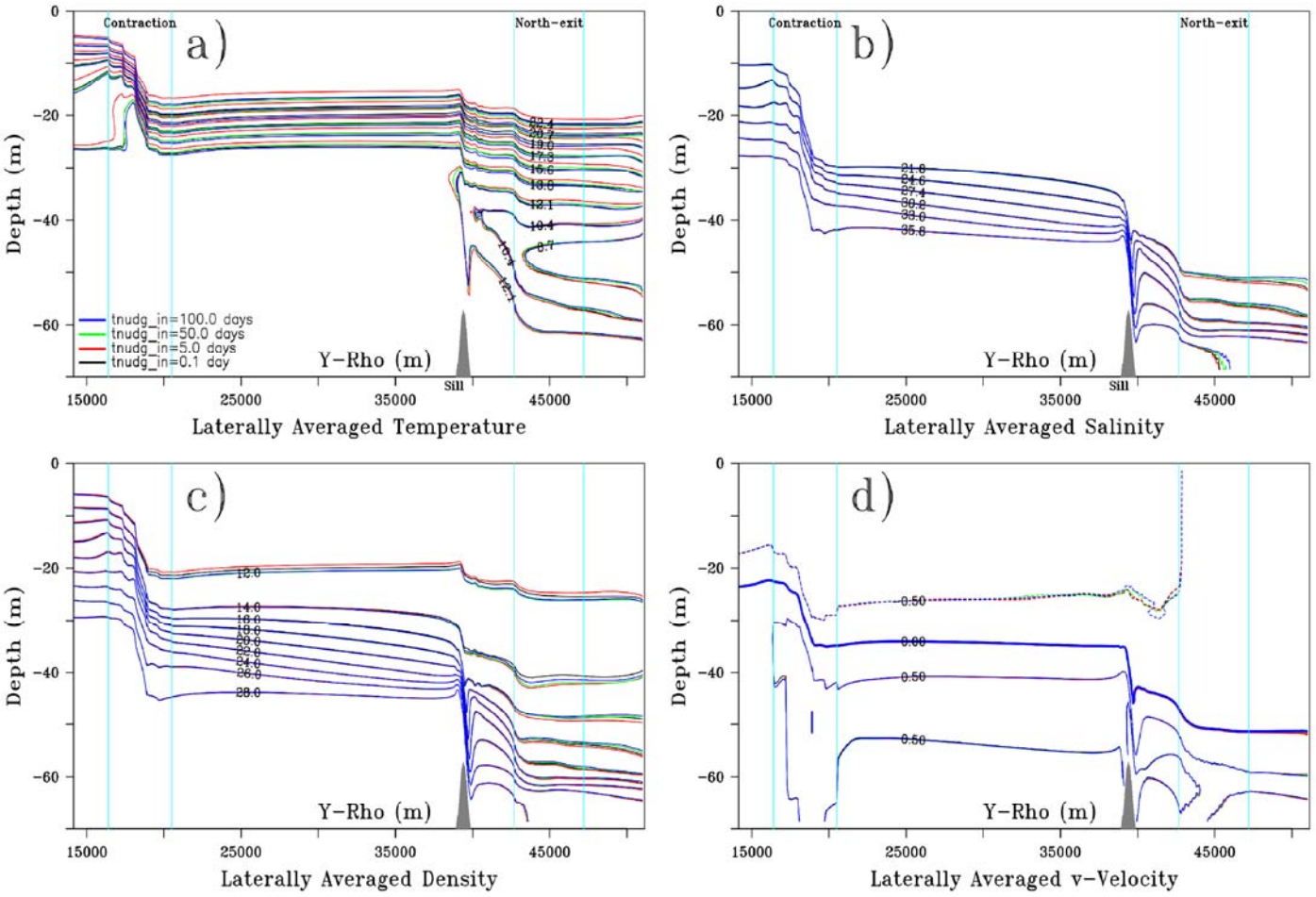

Figure 10. Comparison of the laterally averaged a) temperature, b) salinity c) density and d) v-velocity responses for the four TN01-like experiments of Table 2 with inflowing nudging strength of 0.1 day and outflowing nudging strengths of 0.1, 5.0, 50.0, 100.0 days, location of the topographic changes are marked with light blue lines, same color legends (displayed in the first figure) are used in all figures.

CONCLUSIONS

Being the most hydrodynamically active and constraining element of the Turkish Straits System, Bosphorus Strait has a crucial importance on the exchange between the Mediterranean and Black Seas. Connecting the two large marine basins through a unique maximal-exchange regime created by hydraulic controls through a stratified flow makes the Bosphorus a critical problem to be solved in understanding the response of the entire coupled system. Three-dimensional numerical ocean models are great tools to understand the complex dynamics of the TSS with simplified assumptions in some way or another. Developing standalone models for the elements of TSS are as valuable as the modeling studies aiming to solve the entire TSS.

In this study, a three-dimensional numerical model is applied to an idealized version of the Bosphorus Strait and A CIL-like boundary condition is forced at the Black Sea side with different nudging time-scales. Penetration of a CIL-like stratification can only be achieved by inflowing nudging time-scales less than or equal to one day and the outflowing nudging strength is found to be insignificant.

However, numerical instabilities at the boundary are observed for strong nudging cases with tnudg ≤ 0.01 day suggesting that a careful selection of the inflowing nudging time-scale is important to achieve successful simulations of the CIL even in this highly idealized setup of the Bosphorus Strait.

REFERENCES R

Altıok, H., Sur, H.İ. & Yüce, H. (2012). Variation of the cold intermediate water in the Black Sea exit of the Strait of İstanbul (Bosphorus) and its transfer through the strait. *Oceanologia,* ***54***(2), 233.

Altıok, H. & Kayışoğlu, M. (2015). Seasonal and interannual variability of water exchange in the Strait of Istanbul. *Mediterranean Marine Science,* ***16***(3), 644-655.

Andersen, J.J.E.C. & Carmack, E.C. (1984). Observations of Chemical and Physical Fine-structure in a Strong Pycnoline, Sea of Marmara. *Deep Sea Research*, ***2***, 877-886.

Armi, L. (1986). The hydraulics of two flowing layers with different densities. *Journal of Fluid Mechanics,* ***163***(1), 27-58.

Aydoğdu, A., Pinardi, N., Özsoy, E., Danabasoglu, G., Gürses, Ö. & Karspeck, A. (2018). Circulation of the Turkish Straits System under interannual atmospheric forcing. *Ocean Science,* ***14***, 999-1019.

Beşiktepe, Ş., Özsoy, E., Latif M.A. & Oğuz T. (2000). Marmara Denizi'nin hidrografisi ve Dolaşımı, (Hydrography and Circulation of the Marmara Sea). Marmara Sea 2000 Symposium, İstanbul, Nov. 11-12, 2000, 14 pp. (in Turkish).

Beşiktepe, Ş., Özsoy, E. & Ünlüata, Ü. (1993). Filling of the Marmara Sea by the Dardanelles lower layer inflow. *Deep Sea Research Part I: Oceanographic Research Papers*, ***40***(9), 1815-1838.

Beşiktepe, Ş.T., Sur, H.İ., Özsoy, E., Latif, M.A., Oğuz, T. & Ünlüata, Ü. (1994). The circulation and hydrography of the Marmara Sea. *Progress in Oceanography*, ***34***(4), 285-334.

Dalziel, S.B. (1991). Two-layer hydraulics: a functional approach. *Journal of Fluid Mechanics,* ***223***(1), 135-163.

Defant, A. (1961). Physical Oceanography. Pergamon Press, London, 1961. Vol. 1, pp. xvi + 729; Vol. 2, pp. Viii + 598.

Durski, S.M., Glenn, S.M. & Haidvogel, D.B. (2004). Vertical mixing schemes in the coastal ocean: Comparison of the level 2.5 Mellor-Yamada scheme with an enhanced version of the K profile parameterization. *Journal of Geophysical Research: Oceans*, ***109***(C1).

Farmer, D.M. & Armi, L. (1986). Maximal two-layer exchange over a sill and through the combination of a sill and contraction with barotropic flow. Journal of Fluid Mechanics, ***164***, 53-76.

Garrett, C. & Gerdes, F. (2003). Hydraulic control of homogeneous shear flows. *Journal of Fluid Mechanics,* **475**, 163-172.

Gregg, M.C. & Özsoy, E. (1999). Mixing on the Black Sea shelf north of the Bosphorus. *Geophysical Research Letters*, ***26***(13), 1869-1872

Gregg, M.C. & Özsoy, E. (2002). Flow, water mass changes, and hydraulics in the Bosphorus. *Journal of Geophysical Research: Oceans*, **107**(C3).

Gregg, M.C., Özsoy, E. & Latif, M.A. (1999). Quasi-steady exchange flow in the Bosphorus, *Geophysical Research Letters,* ***26***, 83-86.

Haidvogel, D.B., Arango, H.G., Hedström, K., Beckmann, A., Malanotte-Rizzoli, P. & Shchepetkin, A.F. (2000). Model evaluation experiments in the North Atlantic Basin: simulations in nonlinear terrain-following coordinates. *Dynamics of Atmospheres and Oceans*, ***32***(3), 239-281.

Hedström, K.S. (2009). DRAFT Technical Manual for a Coupled Sea-Ice. *Ocean Circulation Model (Version 3), US Department of the Interior, Mineral Management Service, Anchorage, Alaska, Arctic Region Supercomputing Center, University of Alaska Fairbanks, Contract M07PC13368*.

Helfrich, K.R. (1995). Time-dependent two-layer hydraulic exchange flows. *Journal of Physical Oceanography,* ***25***(3), 359-373.

Hogg, A.M., Ivey, G.N. & Winters, K.B. (2001). Hydraulics and mixing in controlled exchange flows. Journal of Geophysical Research: Oceans (1978-2012), ***106***(C1), 959-972.

Jarosz, E., Teague, W.J., Book, J.W. & Beşiktepe, Ş. (2011a). Observed volume fluxes in the Bosphorus Strait. *Geophysical Research Letters*, ***38***(21).1-6.

Jarosz, E., Teague, W.J., Book, J.W. & Beşiktepe, Ş. (2011b). On flow variability in the Bosphorus Strait. *J. Geophys. Res.,* ***116***, C08038, 1-17. doi:10.1029/2010JC006861.

Jordà, G., Von Schuckmann, K., Josey, S.A., Caniaux, G., García-Lafuente, J., Sammartino, S., Özsoy, E., Polcher, J., Notarstefano, G., Poulain, P-M., Adloff, F., Salat, J., Naranjo, C., Schroeder, K., Chiggiato, J., Sannino, G. & Macías, D. (2016). The Mediterranean Sea heat and mass budgets: Estimates, uncertainties and perspectives. *Progress in Oceanography*, ***156***, 174-208.

Lane-Serff, G.F., Smeed, D.A. & Postlethwaite, C.R. (2000). Multi-layer hydraulic exchange flows. *Journal of Fluid Mechanics,* ***416***, 269-296.

Large, W.G., McWilliams, J.C. & Doney, S.C. (1994). Oceanic vertical mixing: A review and a model with

a nonlocal boundary layer parameterization. *Reviews of Geophysics*, ***32***(4), 363-403.

Latif, M.A., Özsoy, E., Oğuz, T. & Ünlüata, Ü. (1991). Observations of the Mediterranean inflow into the Black Sea. Deep Sea Research Part A. *Oceanographic Research Papers*, ***38***, 711-723.

Marchesiello, P., McWilliams, J.C. & Shchepetkin, A. (2001). Open boundary conditions for long-term integration of regional oceanic models. *Ocean Modelling*, ***3***(1-2), 1-20.

Mellor, G.L. & Yamada, T. (1982). Development of a turbulence closure model for geophysical fluid problems. *Reviews of Geophysics*, ***20***(4), 851-875.

Oğuz, T. (2005). Hydraulic adjustments of the Bosphorus exchange flow. *Geophysical research letters*, ***32***(6). 1-5.

Oğuz, T., Özsoy, E., Latif, M.A., Sur, H.İ. & Ünlüata, Ü. (1990). Modeling of hydraulically controlled exchange flow in the Bosphorus Strait. *Journal of Physical Oceanography*, *20*(7), 945-965.

Orlanski, I. (1976). A simple boundary condition for unbounded hyperbolic flows. *Journal of computational physics*, ***21***(3), 251-269.

Ovchinnikov, I.M. & Popov, Yu.I. (1991). Evolution of the Cold Intermediate Layer in the Black Sea. *Oceanology*, ***27***, 555-560.

Özsoy, E., Latif, M.A., Sur, H.İ, & Goryachkin, Y. (1996). A review of the exchange flow regime and mixing in the Bosphorus strait. *Bulletin-Institut Oceanographique Monaco-Numero Special*, 187-204.

Özsoy, E. & Ünlülata, Ü. (1997). Oceanography of the Black Sea: a review of some recent results. *Earth-Science Reviews,* ***42***(4), 231-272.

Özsoy, E., & Ünlüata, Ü. (1998). The Black Sea, in: A. R. Robinson and K. Brink (editors), The Sea: The Global Coastal Ocean: Regional Studies and Syntheses, 11, John Wiley and Sons, New York, pp. 889-914.

Özsoy, E. (1999). Sensitivity to Global Change in Temperate Euro-Asian Seas (the Mediterranean, Black Sea and Caspian Sea): A Review, in P. Malanotte-Rizzoli and V. N. Eremeev, (editors), The Eastern Mediterranean as a Laboratory Basin for the Assessment of Contrasting Ecosystems, NATO Science Series 2, Environmental Security, 51, Kluwer Academic Publishers, Dordrecht, pp. 281-300.

Özsoy, E., Di Iorio, D., Gregg, M.C. & Backhaus, J.O. (2001). Mixing in the Bosphorus Strait and the Black Sea continental shelf: observations and a model of the dense water outflow. *Journal of marine systems*, ***31***(1), 99-135.

Özsoy, E., Latif, M.A., Beşiktepe, S., Çetin, N., Gregg, M.C., Belokopytov Goryachkin, Y. & Diaconu, V. (1998). The Bosphorus Strait: Exchange Fluxes, Currents and Sea-Level Changes. *NATO Science Series 2 Environmental Security*, ***47***(2), 1-28.

Özsoy, E., Latif, M.A., Tuğrul, S. & Ünlülata, Ü. (1995). Exchanges with the Mediterranean, fluxes, and boundary mixing processes in the Black Sea. Bulletin de l'Institut océanographique, Monaco, Special Number 15, CIESM Science Series No. 1, Monaco 1-25.

Özsoy, E., Oğuz, T., Latif, M.A, Ünlüata, Ü., Sur, H.İ. & Beşiktepe, Ş. (1988). Oceanography of the Turkish Straits - Second Annual Report, Volume I. Physical Oceanography of the Turkish Straits, Institute of Marine Sciences, METU, Erdemli, İçel.

Özsoy, E., Oğuz, T., Latif, M.A. & Ünlüata, Ü. (1986). Oceanography of the Turkish Straits - First Annual Report, Volume I, Physical Oceanography of the Turkish Straits, Institute of Marine Sciences, METU, Erdemli, İçel, Turkey, 223pp.

Öztürk, M., Ayat, B., Aydoğan, B., & Yüksel, Y. (2012). 3D Numerical modeling of stratified flows: case study of the Bosphorus Strait. *Journal of Waterway, Port, Coastal, and Ocean Engineering*, ***138***(5), 406-419.

Pinardi, N. (2009). Misurare il mare: Luigi Ferdinando Marsili nell'Egeo e nel Bosforo, *Bononia University Press*, 1679-1680.

Pratt, L.J. (1986). Hydraulic control of sill flow with bottom friction. *Journal of Physical Oceanography*, ***16***(11), 1970-1980.

Pratt, L.J. (2008). Critical conditions and composite Froude numbers for layered flow with transverse variations in velocity. *Journal of Fluid Mechanics*, ***605***, 281-291.

Raymond, W.H. & Kuo, H.L. (1984). A radiation boundary condition for multi-dimensional flows. *Quarterly Journal of the Royal Meteorological Society*, ***110***(464), 535-551.

Sannino, G., Sözer, A. & Özsoy, E. (2017). A high-resolution modelling study of the Turkish Straits System. *Ocean Dynamics*, ***67***(3-4), 397-432.

Smagorinsky, J. (1963). General circulation experiments with the primitive equations: I. the basic experiment. *Monthly weather review*, ***91***(3), 99-164.

Schroeder, K., Garcìa-Lafuente, J., Josey, S. A., Artale, V., Nardelli, B.B.,Carrillo, A., Gačić, M, Gasparini, G.P., Herrmann, M., Lionello, P.,Ludwig, W., Millot, C., Özsoy, E., Pisacane, G., Sánchez-Garrido, J.C., Sannino, G., Santoleri, R., Somot, S., Struglia, M., Stanev, E.,Taupier-Letage, I., Tsimplis, M.N., Vargas-Yáñez, M., Zervakis, V., Zodiatis,G. (2012). Chapter 3: Circulation of the Mediterranean Seaand its Variability, In: Lionello, P. (ed.), The Climate of

the Mediterranean Region From the past to the future, Elsevier, 592 p

Smeed, D.A. (2000). Hydraulic control of three-layer exchange flows: application to the Bab al Mandab. *Journal of Physical Oceanography*, ***30***(10), 2574-2588.

Soffientino, B. & Pilson. M.E.Q. (2005). The Bosphorus Strait. A special place in the history of Oceanography. *Oceanography*, ***18***(2), 16-23.

Song, Y. & Haidvogel, D. (1994). A semi-implicit ocean circulation model using a generalized topography-following coordinate system. *Journal of Computational Physics*, ***115***(1), 228-244.

Sözer, A. (2013). *Numerical modeling of the bosphorus exchange flow dynamics* (Doctoral dissertation, Ph.D. Thesis, Institute of Marine Sciences, Middle East Technical University, Erdemli, Mersin, Turkey).

Sözer, A. & Özsoy, E. (2002). A three-dimensional model of Bosphorus Strait dynamics. *In The 2nd Meeting on the Physical Oceanography of Sea Straits, Villefranche, 15th-19th April* (pp. 207-210).

Sözer, A. & Özsoy, E. (2017). Modeling of the Bosphorus exchange flow dynamics. *Ocean dynamics*, ***67***(3-4), 321-343.

Stanev, E.V., Grashorn, S. & Zhang, Y.J. (2017). Cascading ocean basins: numerical simulations of the circulation and inter basin exchange in the Azov-Black-Marmara-Mediterranean Seas system. *Ocean Dynamics*, ***67***(8), 1003-1025.

Tolmazin, D. (1985). Changing coastal oceanography of the Black Sea II: Mediterranean effluent. *Progress in oceanography*, 15(4), 277-316.

Tuğrul, S., Beşiktepe, T. & Salihoğlu, I. (2002). Nutrient exchange fluxes between the Aegean and Black Seas through the Marmara Sea. *Mediterranean Marine Science*, ***3***(1), 33-42.

Umlauf, L. & Burchard, H. (2003). A generic length-scale equation for geophysical turbulence models. *Journal of Marine Research*, ***61***(2), 235-265.

Ünlüata, Ü., Oğuz, T., Latif, M.A. & Özsoy, E. (1990). On the physical oceanography of the Turkish Straits. In The physical oceanography of sea straits (pp. 25-60). Springer Netherlands.

Warner, J.C., Sherwood, C.R., Arango, H.G. & Signell, R.P. (2005). Performance of four turbulence closure models implemented using a generic length scale method. *Ocean Modeling*, ***8***(1), 81-113

Wilkin, J.L., Arango, H.G., Haidvogel, D.B., Lichtenwalner, C., Glenn, S.M. & Hedström, K.S. (2005). A regional ocean modeling system for the Long-term Ecosystem Observatory. *Journal of Geophysical Research: Oceans*, ***110***(C6).

Winters, K.B. & Seim, H.E. (2000). The role of dissipation and mixing in exchange flow through a contracting channel. *Journal of Fluid Mechanics*, ***407***, 265-290.

Corresponding author's:
Adil SÖZER
Fatsa Faculty of Marine Sciences, Ordu University, 52400 Turkey
E-mail: adilsozer@odu.edu.tr
ORCID: https://orcid.org/0000-0002-8674-1461